DALTON
FULL PAPER

Antiferromagnetic coupling of transition metal spins across pyrimidine and pyrazine bridges in dinuclear manganese(II), cobalt(II), nickel(II) and copper(II) 1,1,1,5,5,5-hexafluoropentane-2,4-dionate complexes

Takayuki Ishida,*[a] Takashi Kawakami,[b] Shin-ichi Mitsubori,[a] Takashi Nogami,[a] Kizashi Yamaguchi[b] and Hiizu Iwamura[c]

[a] *Department of Applied Physics and Chemistry, The University of Electro-Communications, Chofu, Tokyo 182-8585, Japan. E-mail: ishi@pc.uec.ac.jp*
[b] *Department of Chemistry, Graduate School of Science, Osaka University, Osaka 560-0043, Japan*
[c] *The University of the Air, Wakaba, Mihama-ku, Chiba 261-8586, Japan*

Received 14th March 2002, Accepted 10th June 2002
First published as an Advance Article on the web 11th July 2002

Dinuclear manganese(II), cobalt(II), nickel(II), and copper(II) complexes bridged by pyrimidine and pyrazine derivatives, $L[M(hfac)_2]_2$ [L = 4,6-di(2-pyridyl)pyrimidine (DPPM), 2,3-di(2-pyridyl)pyrazine (DPPZ); M = Mn, Co, Ni, Cu; hfac = 1,1,1,5,5,5-hexafluoropentane-2,4-dionate], were synthesized and their magnetic properties were studied. Antiferromagnetic couplings across the pyrimidine ring were observed for the DPPM complexes with the exchange parameters, $2J/k_B$, of −0.40, −3.1, −9.1 and −46 K for M = Mn, Co, Ni and Cu, respectively. The pyrimidine nitrogen atoms are coordinated at the axial position of each metal ion for M = Mn, Co and Ni, and coordinated equatorially for M = Cu. The DPPZ complexes also exhibited antiferromagnetic interactions, which are weaker than those of the DPPM complexes. Crystal structure analysis indicated that the molecular structures of the four DPPZ complexes are essentially the same in spite of various space groups. *Ab initio* unrestricted Hartree-Fock calculations on $DPPM[Cu(hfac)_2]_2$ predicting a positive effective exchange integral (J) are inconsistent with the experiments, because of overestimation of the role of π-type spin-polarization in DPPM. The J value from the density functional UB3LYP calculations is close to the experimentally determined value, which arises from a σ-type exchange pathway across the pyrimidine ring.

Introduction

Control of magnetic interactions in polynuclear complexes is a key technique for building molecule-based magnets.[1] High-spin organic molecules (**A** and its analogs with spin sources of radicals, carbenes, or nitrenes) are accessible when nonbonding molecular orbitals are present due to π-topological symmetry of the alternant hydrocarbon skeletons.[2] Mataga proposed honeycomb-like high-spin polyradicals and Iwamura modified a model using carbenes (**B**).[3] These model compounds are very attractive but idealistic from the synthetic point of view. Substitution of *m*-phenylene and carbene groups with pyrimidine and transition metal ions, respectively, would make a reaction path more realizable.[4] However, application of the strategy of organic high-spin molecules to transition-metal complexes is not sufficiently understood, and the complexes used for this approach are rare.[4–9] There has been no systematic research on the role of pyrimidine or pyrazine as magnetic couplers before our study.[4]

We have reported the pyrimidine(PM)-bridged dioxovanadium(IV) complex, $PM[VO(hfac)_2]_2$ (hfac = 1,1,1,5,5,5-hexafluoropentane-2,4-dionate), with a ground triplet state (**C**).[10,11] The dπ character of vanadium(IV) spins is supposed to be crucial for ferromagnetic coupling.[11] The oxovanadium oxygen atom can work as a cap which occupies an axial position and accordingly facilitates exclusive preparation of dinuclear compounds using bis(hfac) metal salts. We designed another type of PM-bridged complex $L[M(hfac)_2]_2$ as a dinuclear prototype, in which two 2-pyridyl groups are introduced at the 4- and 6-positions on PM as a cap. Thus, target compounds have two $(bpy)M(hfac)_2$-type coordination structures (bpy denotes 2,2′-bipyridyl) which are connected by the 1,3-μ-PM ligand, and the octahedral coordination sites of each metal ion are occupied with N_2O_4 atoms from three bidentate ligands.

We preliminarily reported the antiferromagnetic interactions of these dinuclear Mn, Co, Ni and Cu complexes with L = 4,6-di(2-pyridyl)pyrimidine (DPPM)[4] (for the molecular structures, see below). In this article, we describe the X-ray crystal structures of the DPPM-bridged complexes and discuss a mechanism of antiferromagnetic exchange coupling across the PM bridges. We also compare their molecular structures and magnetic properties with those of the corresponding pyrazine (PZ) derivatives $L[M(hfac)_2]_2$ [L = 2,3-di(2-pyridyl)pyrazine) (DPPZ)]. The complexes investigated in the present work are abbreviated as **DPPM–M** and **DPPZ–M** hereafter, in which **M** denotes the hfac salts of divalent transition metal ions (Mn, Co, Ni and Cu).

In addition to the experimental studies, our theoretical treatments enable us to investigate magnetic properties and gain insight into exchange mechanisms. *Ab initio* unrestricted Hartree-Fock (UHF) and density functional (DFT) calculations were carried out for the **DPPM–Cu** molecule. The calculation includes all of the atoms and the atomic positions determined by the X-ray diffraction study. Disagreement between two calculations will be discussed.

DOI: 10.1039/b202635j

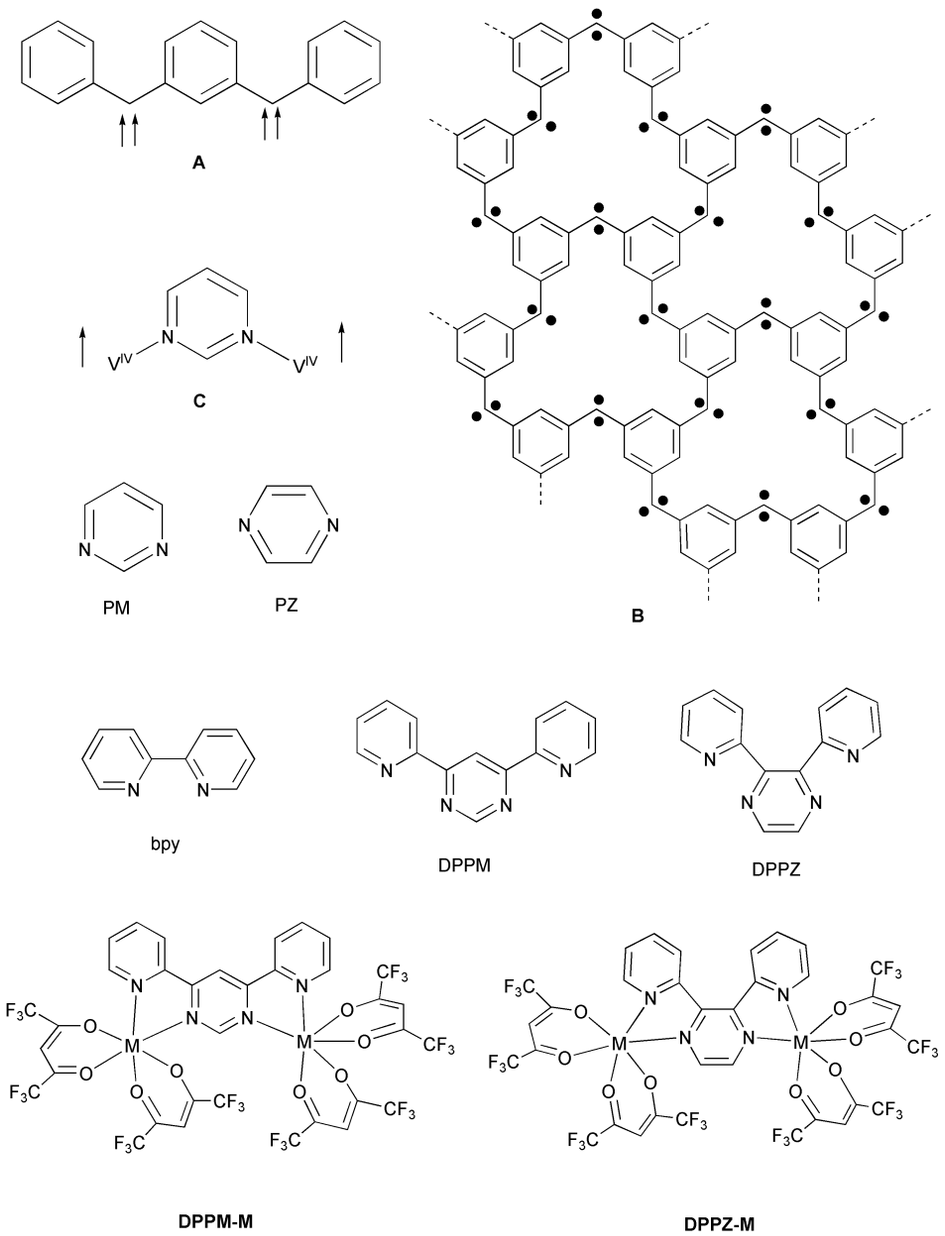

Experimental

Materials

The hfac salts of Mn^{II}, Co^{II}, Ni^{II} and Cu^{II} were purchased from Tokyo Chemical Industry. The DPPZ ligand was purchased from Aldrich. They were used without further purification. The DPPM ligand was prepared according to the literature method.[12] Typical procedures of the preparation of **DPPM–** and **DPPZ–M** are as follows.

A chloroform solution (5 mL) containing the bridging ligand (23 mg, 0.1 mmol) was added to a solution of $M(hfac)_2$ (*ca.* 0.1 g, 0.2 mmol) in a 4 : 1 chloroform–methanol mixed solvent (5 mL). After refluxing for 1 h, the mixture was concentrated to *ca.* 5 mL by a rotary evaporator. The crude product of the complex was crystallized after standing at room temperature and collected on a filter. For the preparation of **DPPM–Mn**, chloroform and diethyl ether were used as a solvent. For the preparation of **DPPM–Cu**, chloroform was used as a solvent, and the complexation was conducted at room temperature because the green microcrystalline product appeared immediately after mixing two chloroform solutions. The specimens suitable for elemental analysis, X-ray crystallographic analysis, and magnetic study were purified by repeated recrystallization.

Table 1 summarizes the yields, crystallization solvents, elemental analysis for the complexes obtained here. The elemental analysis and X-ray diffraction study indicate that the **DPPM–M** crystals contain a half mole of benzene as a crystal solvent.[13] Two types of the crystals of **DPPZ–Mn** were found, benzene-solvated and non-solvated forms. The former gave a good single crystal, which was suitable for X-ray crystallographic analysis.

X-Ray crystallographic analysis

Diffraction data were collected on a Rigaku R-axis RAPID diffractometer with graphite monochromated MoKα radiation ($\lambda = 0.71069$ Å) at 100 K, unless otherwise noted. The data were collected at 220 and 190 K for **DPPZ–Ni** and **–Cu**, respectively, because micro cracks occurred on cooling down to lower temperatures. The structures were directly solved by a heavy-atom Patterson method in the teXsan program package.[14] Numerical absorption correction was used. All of the hydrogen atoms could be found in difference Fourier maps, and the parameters of the hydrogen atoms were included in the refinement. The thermal displacement parameters were refined anisotropically for non-hydrogen atoms and isotropically for hydrogen atoms. Full-matrix least-squares methods were applied using all of the unique diffraction data.

Table 1 Yields, melting points, and elemental analyses of **DPPM–** and **DPPZ–M** (M = Mn, Co, Ni and Cu)

Compound	Yield (%)[a]	Mp/°C	Recryst. solv.	Anal.[b] C (%)	H (%)	N (%)
DPPM–Mn·0.5C_6H_6	36[c]	263(dec)	C_6H_6–CH_3OH	35.45 (36.69)	1.33 (1.41)	4.26 (4.63)
DPPM–Co·0.5C_6H_6	18	288(dec)	C_6H_6–CH_3OH	35.93 (36.45)	1.46 (1.41)	4.94 (4.60)
DPPM–Ni·0.5C_6H_6	76	305(dec)	C_6H_6–CH_3OH–CH_3COCH_3	36.29 (36.46)	1.62 (1.41)	5.01 (4.60)
DPPM–Cu·0.5C_6H_6	20[d]	217(dec)	C_6H_6–CH_3OH	35.57 (36.17)	1.41 (1.40)	4.63 (4.56)
DPPZ–Mn	53	159–161	$CHCl_3$–*n*-C_6H_{14}	33.22 (34.83)	1.34 (1.20)	4.19 (4.78)
DPPZ–Co	60	221–223	$CHCl_3$–*n*-C_6H_{14}	34.56 (34.60)	1.35 (1.20)	5.00 (4.75)
DPPZ–Ni	66	253–254	$CHCl_3$–CH_3OH	34.63 (34.61)	1.33 (1.20)	5.04 (4.75)
DPPZ–Cu	21	80–83	CH_2Cl_2–*n*-C_6H_{14}	34.25 (34.33)	1.37 (1.19)	4.83 (4.71)

[a] All the complexations were carried out in a refluxing chloroform–methanol mixed solvent for 1 h, unless otherwise noted. [b] Calculated values in parentheses. [c] In chloroform–diethyl ether. [d] In chloroform at room temperature.

There are two conformations for each trifluoromethyl group as indicated by electron densities in difference Fourier maps and by elongated thermal ellipsoids of fluorine atoms even at 100 K. Disorder models were applied for trifluoromethyl groups belonging to C20 and C24 in **DPPM–Mn**, C25, and C34 in **DPPZ–Ni**, and C19, C25, and C34 in **DPPZ–Cu**, which appreciably improved the refinement. Tables 2 and 3 summarize the selected crystallographic data of **DPPM–** and **DPPZ–M**, respectively.

CCDC reference numbers 180719–180726.

See http://www.rsc.org/suppdata/dt/b2/b202635j/ for crystallographic data in CIF or other electronic format.

Magnetic measurements

Magnetic susceptibilities were measured on a Quantum Design MPMS SQUID magnetometer at 0.5 T in a temperature range down to 1.8 K. The magnetic responses were corrected with diamagnetic blank data of the sample holder obtained separately. The diamagnetic contribution of the sample itself was estimated from Pascal's constants.

Molecular orbital calculations

Molecular orbital calculations were employed using unrestricted Hartree-Fock (UHF) and unrestricted density functional (DFT) UBLYP (Becke–Lee–Yang–Parr) methods in the Gaussian98 program packages.[15] UB2LYP (half-and-half) and UB3LYP[16] methods were also used for hybrid methods between HF and DFT. The basis set (3333/33/3) and diffuse and polarized functions were applied for Cu and 4–31G for the other atoms. In this expression '3' means that three primitive Gaussian-type functions are used for one constructed function. Here, four s-type, two p-type, and one d-type functions are considered, which are applied to the electron configuration of the Cu atom, *i.e.*, (1s, 2s, 3s, 4s), (2p, 3p), and (3d). The atomic positions were available from the X-ray crystallographic analysis.

Results

Structures of DPPM– and DPPZ–M

The crystal structures of **DPPM–M** (M = Mn, Co, Ni and Cu) are isomorphous and the molecular structure and atomic numbering of **DPPM–Co** are shown in Fig. 1(a). The atoms of **DPPM–Mn**, **Ni** and **Cu** are similarly numbered. Selected

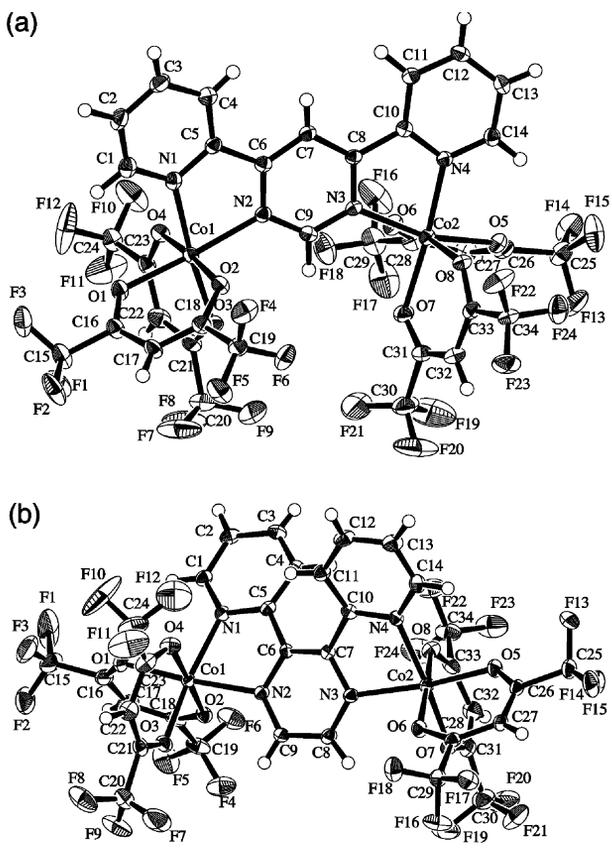

Fig. 1 Ortep drawings of **DPPM–Co** (a) and **DPPZ–Co** (b) with thermal ellipsoids at the 50% probability level. Atomic numberings are also shown.

bond distances and angles of **DPPM–M** are listed in Table 4. Although the two metal ions M1 and M2 are crystallographically independent, the coordination spheres of M1 and M2 are similar to each other; the molecule has a pseudo-C_2 symmetry with respect to the C7–C9 axis. The crystal consists of a racemate of Δ–Δ and Λ–Λ enantiomers, which are related by an inversion symmetry in the $P\bar{1}$ space group. The DPPM moieties are almost planar as indicated by small torsion angles (< 4°) around the C5–C6 and C8–C10 bonds.

Several intermolecular F ··· F contacts are found, but these contacts can hardly afford any appreciable magnetic exchange pathways. Furthermore, benzene molecules reside in the middle

Table 2 Crystallographic data for **DPPM–M**·0.5C_6H_6 (M = Mn, Co, Ni and Cu)

M	Mn	Co	Ni	Cu
Formula	$C_{37}H_{17}N_4O_8F_{24}Mn_2$	$C_{37}H_{17}N_4O_8F_{24}Co_2$	$C_{37}H_{17}N_4O_8F_{24}Ni_2$	$C_{37}H_{17}N_4O_8F_{24}Cu_2$
Habit	Orange needles	Red needles	Green needles	Green needles
Dimensions/mm	0.4 × 0.12 × 0.12	0.43 × 0.18 × 0.15	0.65 × 0.40 × 0.15	0.25 × 0.20 × 0.08
T/K	100	100	100	100
Crystal system	Triclinic	Triclinic	Triclinic	Triclinic
Space group	$P\bar{1}$	$P\bar{1}$	$P\bar{1}$	$P\bar{1}$
a/Å	14.012(3)	13.8200(5)	13.943(2)	13.649(2)
b/Å	15.195(4)	15.0112(7)	15.060(2)	15.335(2)
c/Å	11.832(2)	11.7748(6)	11.682(2)	11.875(1)
α/° [a]	96.148(10)	95.758(1)	95.441(7)	95.023(6)
β/° [a]	88.615(5)	89.758(1)	91.207(7)	99.372(4)
γ/° [a]	113.49(1)	114.153(2)	114.168(3)	111.435(2)
V/Å^3	2296.5(8)	2215.8(2)	2223.1(5)	2253.3(4)
Z	2	2	2	2
D_{calc}/g cm^{-3}	1.752	1.827	1.821	1.811
Unique data for refinement	9865	9757	9655	9617
μ(Mo-Kα)/mm^{-1}	0.701	0.906	1.003	1.098
R (F) [b] ($I > 2\sigma(I)$)	0.0578	0.0462	0.0539	0.0621
R_w(F^2) [c] (all data)	0.163	0.147	0.169	0.180
G.O.F.	1.43	1.47	1.46	1.39

[a] The cell parameters are transformed for the sake of comparison. These angles are conventionally taken to be α = 96.148(10), β = 91.385(5), γ = 66.51(1)° for M = Mn and α = 95.758(1), β = 90.242(1), γ = 65.847(2)° for M = Co. [b] $R = \Sigma||F_o| - |F_c||/\Sigma|F_o|$. [c] $R_w = [\Sigma w(F_o^2 - F_c^2)^2/\Sigma w(F_o^2)^2]^{1/2}$.

Table 3 Crystallographic data for **DPPZ–M**·(solvent) (M = Mn, Co, Ni and Cu)

M	Mn	Co	Ni	Cu
Formula	$C_{40}H_{20}N_4O_8F_{24}Mn_2$	$C_{34}H_{14}N_4O_8F_{24}Co_2$	$C_{34}H_{14}N_4O_8F_{24}Ni_2$	$C_{34}H_{14}N_4O_8F_{24}Cu_2$
Habit	Orange platelets	Red blocks	Blue blocks	Green blocks
Dimensions/mm	0.35 × 0.35 × 0.10	0.50 × 0.35 × 0.15	0.35 × 0.15 × 0.15	0.26 × 0.23 × 0.10
T/K	100	100	220	190
Crystal system	Triclinic	Monoclinic	Monoclinic	Monoclinic
Space group	$P\bar{1}$	$P2_1/n$	$P2_1/c$	$P2_1/c$
a/Å	13.180(2)	13.1827(4)	13.6123(7)	13.9013(5)
b/Å	14.202(2)	13.0002(4)	19.486(1)	18.4749(6)
c/Å	13.163(1)	24.7946(8)	16.861(1)	17.4447(6)
α/°	100.171(2)	90	90	90
β/°	94.470(6)	98.895(1)	98.962(4)	99.128(1)
γ/°	72.635(3)	90	90	90
V/Å^3	2313.9(5)	4198.1(2)	4417.7(5)	4423.5(3)
Z	2	4	4	4
D_{calc}/g cm^{-3}	1.795	1.867	1.774	1.786
Unique data for refinement	9718	9518	8574	9146
μ(Mo-Kα)/mm^{-1}	0.699	0.952	1.006	1.115
R (F) [a] ($I > 2\sigma(I)$)	0.0538	0.0544	0.0618	0.0481
R_w(F^2) [b] (all data)	0.174	0.155	0.197	0.145
G.O.F.	1.47	1.45	0.999	0.973

[a] $R = \Sigma||F_o| - |F_c||/\Sigma|F_o|$. [b] $R_w = [\Sigma w(F_o^2 - F_c^2)^2/\Sigma w(F_o^2)^2]^{1/2}$.

of two molecules of **DPPM–M** as a crystal solvent, and π-electron systems of bridging ligands are considerably separated from a neighboring molecule. Thus, each molecule should be magnetically isolated.

We focus our attention on detailed geometries around the metal ions and especially around M1–N2 and M2–N3 bonds which provide the main exchange pathway. The M–N bond lengths decrease in the order of M = Mn, Co, Ni and Cu (Table 4). The M–N distances are much longer than M–O distances in **DPPM–Mn** and **–Co**, indicating that the pyrimidine N2 and N3 atoms are coordinated at axial positions. Since the M1–N2 and M2–N3 distances are only slightly longer than other bonds for **DPPM–Ni**, the geometrical assignment of the Mn and Co complexes may hold for the Ni complex. On the other hand, the M1–O2 and M1–O4 distances are longer than those of M1–O1, –O3, –N1, and –N2 for **DPPM–Cu**, indicating that the nitrogen atoms are equatorially coordinated.

The crystals of **DPPZ–M** (M = Mn, Co, Ni and Cu) have various space groups, but the molecular structures are essentially identical to each other. The molecular structure and atomic numbering of **DPPZ–Co** are shown in Fig. 1(b). The atoms in the Mn, Ni, and Cu complexes are similarly numbered. Selected bond distances and angles of **DPPZ–M** are listed in Table 5. Owing to the steric hindrance, the DPPZ moieties are largely twisted by angles of 17–39° around the C5–C6 and C7–C10 bonds. Each molecule has a Δ–Δ or Λ–Λ conformation, and the enantiomers are related by an inversion symmetry in the centrosymmetric space groups.

Similarly to the DPPM complexes, the pyrazine nitrogen atoms (N2 and N3) are coordinated from the axial directions for **DPPZ–Mn**, **–Co**, and **–Ni** (Table 5). As described in the Experimental section, the crystals of **DPPZ–Ni** and **–Cu** lost their transparency on cooling below *ca.* 220 and 190 K, respectively, strongly suggesting that a structural phase transition took place. Actually, the cell constants at 100 K are somewhat different from those at 220 and 190 K.[17]

Magnetic properties

Fig. 2 shows the temperature dependence of the $\chi_{mol}T$ product per molecule for **DPPM–M**. The $\chi_{mol}T$ values at 300 K indicate that each metal ion has a high-spin state. The $\chi_{mol}T$ values

Table 4 Selected bond lengths (Å) and angles (°) for **DPPM–M**·$0.5C_6H_6$ (M = Mn, Co, Ni and Cu)

M	Mn	Co	Ni	Cu
M1–O1	2.161(2)	2.074(2)	2.048(2)	1.933(2)
M1–O2	2.179(2)	2.068(2)	2.045(2)	2.250(3)
M1–O3	2.157(3)	2.049(2)	2.034(3)	1.966(3)
M1–O4	2.138(2)	2.046(2)	2.029(2)	2.414(3)
M1–N1	2.243(3)	2.106(2)	2.063(3)	2.001(3)
M1–N2	2.272(3)	2.121(2)	2.079(3)	2.001(3)
M2–O5	2.132(3)	2.044(2)	2.027(2)	2.020(3)
M2–O6	2.154(2)	2.053(2)	2.027(2)	2.326(3)
M2–O7	2.129(3)	2.051(2)	2.027(2)	1.938(3)
M2–O8	2.195(2)	2.087(2)	2.061(2)	2.211(3)
M2–N3	2.297(3)	2.136(2)	2.096(3)	2.035(3)
M2–N4	2.253(3)	2.109(2)	2.067(3)	1.989(3)
O1–M1–O2	83.56(9)	87.40(8)	89.24(9)	87.37(10)
O3–M1–O4	82.11(10)	87.21(8)	89.55(10)	83.1(1)
N1–M1–N2	72.9(1)	77.20(9)	79.3(1)	80.7(1)
O5–M2–O6	83.33(9)	87.76(8)	89.89(9)	81.9(1)
O7–M2–O8	82.92(9)	86.88(8)	88.69(9)	87.1(1)
N3–M2–N4	72.2(1)	76.61(8)	78.8(1)	80.6(1)
N1–C5–C6–N2	−.0(4)	−2.9(3)	−1.6(4)	−0.5(4)
N3–C8–C10–N4	−4.1(4)	−1.8(3)	0.3(4)	−4.0(4)

Table 5 Selected bond lengths (Å) and angles (°) for **DPPZ–M** (M = Mn, Co, Ni and Cu)

M	Mn	Co	Ni	Cu
M1–O1	2.106(2)	2.052(3)	2.030(4)	1.967(2)
M1–O2	2.163(2)	2.042(3)	2.017(3)	2.224(2)
M1–O3	2.121(2)	2.070(3)	2.036(4)	1.976(3)
M1–O4	2.197(2)	2.067(3)	2.026(4)	2.217(2)
M1–N1	2.227(3)	2.105(3)	2.051(4)	1.998(3)
M1–N2	2.280(3)	2.132(3)	2.070(4)	2.031(3)
M2–O5	2.121(2)	2.026(3)	2.014(3)	2.169(2)
M2–O6	2.155(2)	2.052(3)	2.014(3)	1.960(2)
M2–O7	2.135(2)	2.056(3)	2.024(4)	1.967(2)
M2–O8	2.151(2)	2.078(3)	2.026(4)	1.960(2)
M2–N3	2.284(3)	2.134(3)	2.136(4)	2.455(3)
M2–N4	2.242(3)	2.112(3)	2.076(4)	2.037(3)
O1–M1–O2	82.21(9)	88.9(1)	90.8(1)	87.95(9)
O3–M1–O4	81.11(9)	86.6(1)	88.7(2)	85.6(1)
N1–M1–N2	72.43(10)	77.2(1)	79.2(2)	80.1(1)
O5–M2–O6	83.10(9)	88.9(1)	90.8(1)	89.25(8)
O7–M2–O8	82.90(9)	86.0(1)	89.6(1)	90.62(10)
N3–M2–N4	72.04(10)	77.0(1)	78.5(2)	74.87(10)
N1–C5–C6–N2	25.7(4)	18.3(4)	23.3(6)	16.8(4)
N3–C7–C10–N4	19.4(4)	23.1(4)	28.2(6)	38.8(4)

dominantly decrease with decreasing temperature for all of the complexes investigated here, clearly indicating that the spins of the metal ions are antiferromagnetically coupled; namely, the dinuclear molecules have a low-spin ground state. Since the X-ray crystal structure analysis indicates that no appreciable interatomic contacts were found among the molecules, the magnetic interaction should be attributed to the intramolecular coupling.

We analyzed these data by the dinuclear models as expressed by eqn. 1, on the basis of the conventional van Vleck equation for Heisenberg spins.[1,18] The spin Hamiltonian is defined by $H = -2JS_i \cdot S_j$.

$$\chi_{\mathrm{mol}} = \frac{2Ng^2\mu_{\mathrm{B}}^2}{k_{\mathrm{B}}T} \frac{e^{-2x} + 5Ae^{-6x} + 14Be^{-12x} + 30Ce^{-20x} + 55De^{-30x}}{1 + 3e^{-2x} + 5Ae^{-6x} + 7Be^{-12x} + 9Ce^{-20x} + 11De^{-30x}} \quad (1)$$

where $x = -J/k_{\mathrm{B}}T$.

The parameters *A*–*D* should be set as follows. $A = B = C = D = 0$ for $S = 1/2$ (M = Cu(II)); $A = 1$ and $B = C = D = 0$ for $S = 1$ (M = Ni(II)); $A = B = 1$ and $C = D = 0$ for $S = 3/2$ (M = Co(II)); $A = B = C = D = 1$ for $S = 5/2$ (M = Mn(II)).

Table 6 Best fit parameters for **DPPM–** and **DPPZ–M** (M = Mn, Co, Ni and Cu)

Compound	*g*	$2J(k_{\mathrm{B}}^{-1})$/K
DPPM–Mn·$0.5C_6H_6$	2.07	−0.40
DPPM–Co·$0.5C_6H_6$	~2.69	~−3.1
DPPM–Ni·$0.5C_6H_6$	2.30	−9.1
DPPM–Cu·$0.5C_6H_6$	2.29	−46
DPPZ–Mn	2.00	−0.34
DPPZ–Mn·C_6H_6	2.00	−0.40
DPPZ–Co	~2.6	[a]
DPPZ–Ni	2.19	−1.19
DPPZ–Cu	2.12	<0.1

[a] The data did not obey the Heisenberg–van Vleck equation.

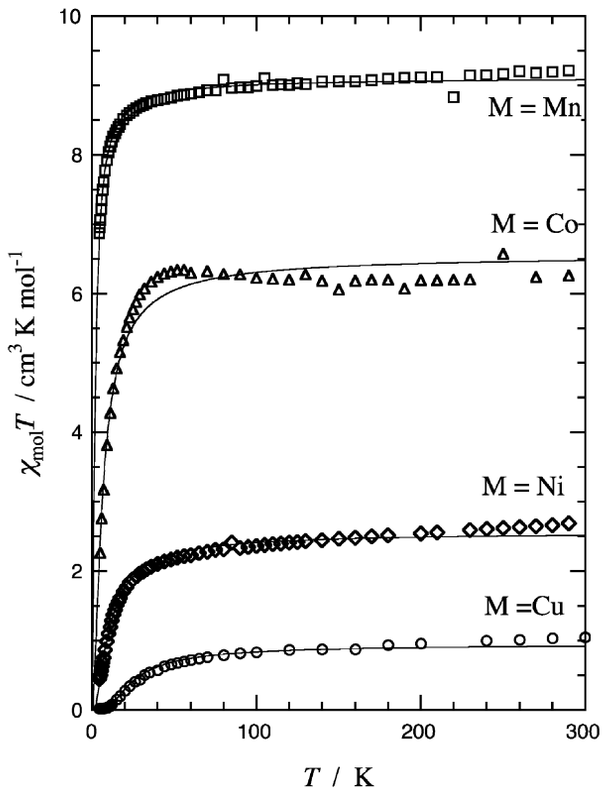

Fig. 2 Temperature dependence of the product $\chi_{\mathrm{mol}}T$ for **DPPM–Mn**, **Co**, **Ni** and **Cu**. The solid lines represent the fits to the equation based on the dinuclear model.

We have to take into account the contribution of angular momentum for the cobalt(II) (d^7) complexes and the van Vleck treatment may give approximate results. Indeed, the $\chi_{\mathrm{mol}}T$ vs. T plots of **DPPM–** and **DPPZ–Co** show somewhat anomalous behavior, which cannot be explained by spin–spin coupling alone. On the other hand, manganese(II) (d^5), nickel(II) (d^8), and copper(II) (d^9) complexes usually have negligible contribution of angular momentum, and obey the Heisenberg–van Vleck model.

The optimized parameters are listed in Table 6, and theoretical curves with these parameters are superposed in Fig. 2. The negative *J* values imply that the two metal spins are antiferromagnetically correlated. A significantly large antiferromagnetic interaction ($2J/k_{\mathrm{B}} = -46$ K) was observed for **DPPM–Cu**, where the singlet–triplet energy gap corresponds to 2*J*. In sharp contrast to *m*-phenylene-bridged diradicals and dicarbenes (**A**) having a high-spin ground state, the present work unequivocally demonstrates that **DPPM–Cu**

has a singlet ground state. Antiferromagnetic couplings have also been reported in other PM-bridged copper(II) complexes.[19–21]

The $\chi_{mol}T$ vs. T plots for **DPPM–Mn** and **–Ni** also fit well to the dinuclear model equations, as indicated by the calculated curves (Fig. 2). Antiferromagnetic couplings are observed regardless of the different coordination basal planes in **DPPM–Mn**, **Co**, **Ni** and **Cu**. In the case of **DPPM–Co**, the $\chi_{mol}T$ value increases on cooling, reaches to a broad maximum, and finally decreases. The increase of $\chi_{mol}T$ may be attributed to the contribution of angular momentum of the cobalt spins. A similar broad maximum is observed in the measurements on **DPPZ–Co** (see below). These broad maxima seem to result from the same origin but a sharp decrease at low temperature was observed only for **DPPM–Co**. The negative J value of **DPPM–Co** was estimated, considering the final decrease to be important.

Magnetic measurements on the **DPPZ–M** series may afford a good comparison of the role of exchange couplers in the isomeric pyrimidine and pyrazine bridges. Fig. 3 shows the

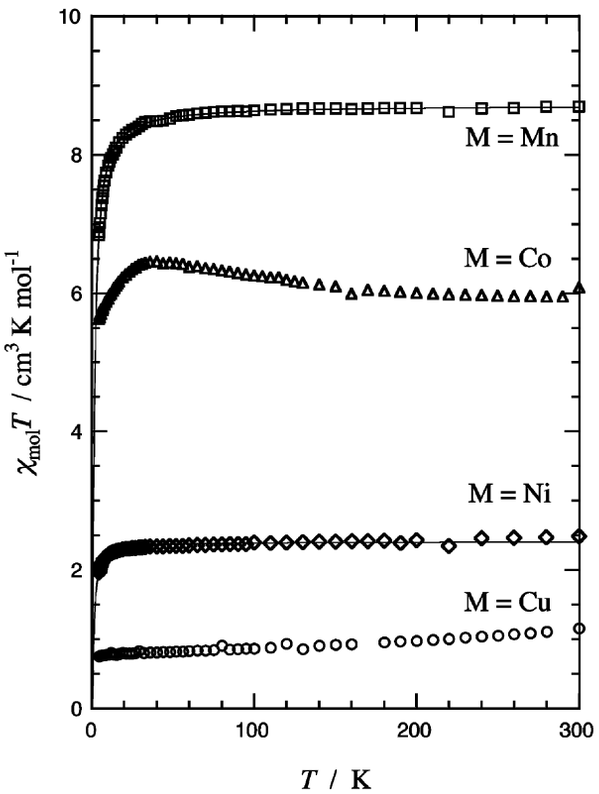

Fig. 3 Temperature dependence of the product $\chi_{mol}T$ for **DPPZ–Mn**, **Co**, **Ni** and **Cu**. The solid lines represent the fits to the equation based on the dinuclear model.

temperature dependence of the $\chi_{mol}T$ values for the DPPZ-bridged complexes. We obtained two forms of the crystals of **DPPZ–Mn** with and without solvated benzene molecules. Their magnetic properties were essentially identical to each other and the optimized parameters of **DPPZ–Mn**·C_6H_6 are also listed in Table 6. This supports the magnetic interactions obtained here being ascribed as intramolecular in nature.

The parameter of magnetic interaction in **DPPZ–Co** could not be determined, but from the comparison of the decreases of $\chi_{mol}T$ in the low temperature region in **DPPM–** and **DPPZ–Co** we can assume that **DPPZ–Co** has a smaller $|J|$ than **DPPM–Co**. The exchange parameter for **DPPZ–Ni** was determined by the theoretical fit. The complex **DPPZ–Cu** has practically no interaction.[17] The absolute J values of **DPPZ–Co**, **–Ni**, and **–Cu** are smaller than those of the corresponding DPPM complexes. On the other hand, **DPPM–** and **DPPZ–Mn** have comparable J values.

Table 7 Effective exchange integrals (J_{ab}) and spin densities calculated from *ab initio* UHF and DFT (UB2LYP, UB3LYP and UBLYP) methods for **DPPM–Cu**

Method	UHF	UB2LYP	UB3LYP	UBLYP
J_{ab}(X)[a]/cm^{-1}	144.9	−6.9	−16.7	−66.1
J_{ab}(AP–X)[a]/cm^{-1}	120.2	−6.9	−16.6	−64.0
Spin densities for the most stable spin state[b]				
Cu1	0.896	0.700	0.515	0.406
N2	0.338	0.049	0.055	0.052
C9	−0.348	0.002	0.001	0.001
N3	0.350	−0.061	−0.068	−0.066
Cu2	0.893	−0.699	−0.519	−0.414
N1	0.176	0.088	0.091	0.086
O1	0.018	0.058	0.106	0.124
O2	0.002	0.005	0.011	0.010
O3	0.032	0.096	0.155	0.168
O4	−0.005	0.003	0.014	0.031

[a] J_{ab}(X) and J_{ab}(AP–X) are effective exchange integrals without and with spin projection, respectively. [b] High- and low-spin states for UHF and DFT calculations, respectively.

We should briefly report on magnetic properties of mononuclear complexes. We also prepared the complexes (bpy)-M(hfac)$_2$ (M = Mn, Co, Ni and Cu; abbreviated as **BPY–M**).The temperature dependence of the magnetic susceptibility for **BPY–Mn** and **–Cu** simply obey the Curie law (C = 4.38 and 0.436 cm^3 K mol^{-1}, respectively). A negligible Weiss temperature was obtained for **BPY–Ni** from the Curie–Weiss equation (C = 1.20 cm^3 K mol^{-1} and θ = −0.1 K). These findings support intermolecular interactions being neglected when bulky hfac ligands prevent intermolecular contacts, and also the temperature dependence observed for **DPPM–** and **DPPZ–M** can be attributed to the spin–spin interaction and not to any contribution of mononuclear origin (*e.g.*, zero-field splitting). Since **BPY–Co** does not obey the Curie–Weiss law, it seems difficult to determine precisely the exchange parameters for **DPPM–** and **DPPZ–Co**.

Molecular orbital calculations

We employed *ab initio* unrestricted Hartree-Fock (UHF) calculations and density functional (DFT) UBLYP, UB2LYP and UB3LYP calculations for evaluation of the exchange parameter J and spin distribution on the ligand in **DPPM–Cu**. Table 7 shows the J_{ab} values obtained by the above computational methods. Here, J_{ab}(X) and J_{ab}(AP–X) imply effective exchange integrals without and with spin projection to reduce spin contamination, respectively. The following conclusions are extracted from Table 7:

(1) The UHF method gave a positive J_{ab} value and large ferromagnetic interaction is expected between two Cu atoms. The UHF calculation is inconsistent with the experimental results. (2) The J_{ab} values calculated by UB3LYP are −16.6 cm^{-1} for **DPPM–Cu**. This value corresponds to $2J/k_B$ = −46.3 K, which is very close to the experimental value (Table 6). (3) All of the DFT methods give negative J_{ab} values and the absolute values increase in the order UB2LYP < UB3LYP < UBLYP. The difference between J_{ab}(X) and J_{ab}(AP–X) values is very small and accordingly the spin contamination is small. (4) The nitrogen atoms (N1 and N2) carry positive spin densities for all calculation methods. (5) The UHF calculation gave large spin densities on the PM ring.

DFT methods have been shown to give good agreement with spin densities derived from polarized neutron diffraction[22] and NMR[23] experiments and also to give good estimates of magnetic interactions.[24] In the present study, the DFT UB3LYP calculations reproduced well the experimental magnetic interactions in **DPPM–Cu**. Fig. 4(b) and 4(c) illustrate the spin densities for the ground states calculated by UHF (high-spin) and

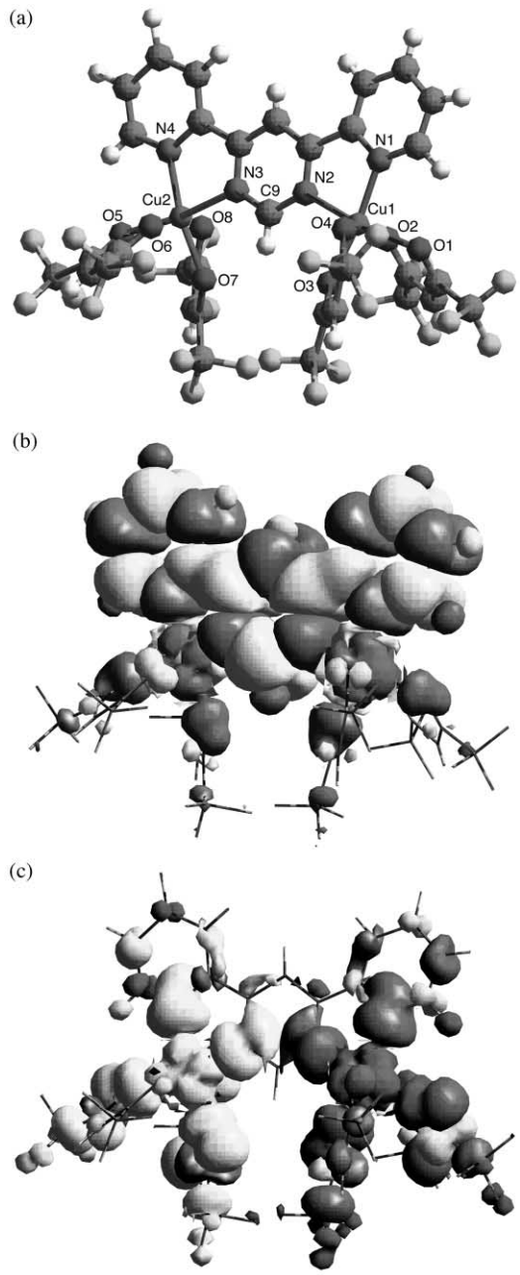

Fig. 4 Calculated spin density distribution at the most stable spin state of **DPPM–Cu** with the surface threshold level of 0.001. (a) Structure of the calculated molecule. (b) Calculation by the *ab initio* UHF method. (c) Calculation by the UB3LYP method. For details of the calculations, see the text.

UB3LYP (low-spin), respectively. The regions of up (alpha) and down (beta) densities are shown in dark and light gray colors, respectively, and the cut-off threshold is set to be 0.001. Fig. 4(a) depicts the skeleton of the molecule. The total spin densities condensed on each atom are also listed in Table 7.

Discussion

We have reported that the PM- and PZ-bridged dinuclear oxovanadium complexes exhibit intramolecular ferro- and antiferromagnetic interactions, respectively,[11] being in good agreement with the spin-polarization mechanism as in organic compounds. The electron configuration of vanadium(IV) is d^1 (t_{2g}^1) which affords a π-type symmetry around a metal–ligand bond and the dπ–pπ orbital overlap between the metal and coordinated atoms is essential for realization of ferromagnetic interaction.[11] In the present study, however, both PM and PZ bridges play the role of antiferromagnetic coupler. The d electron configuration, especially dσ (e_g) spins which Mn^{II}, Co^{II}, Ni^{II} and Cu^{II} ions possess in the present complexes, seems to be crucial for the magnetic interaction.

The coordination geometry (axial or equatorial) is also very important, as suggested by the following instance. Two types of polymeric copper(II) nitrate complexes have been reported: ferromagnetic $[PM_2{\cdot}Cu(NO_3)_2]_n$ and antiferromagnetic $[PM{\cdot}Cu(NO_3)_2{\cdot}(H_2O)_2]_n$.[19] The former has axial coordination at one nitrogen atom of PM and equatorial coordination at the other (axial–equatorial, see Scheme 1). An equatorial–equatorial

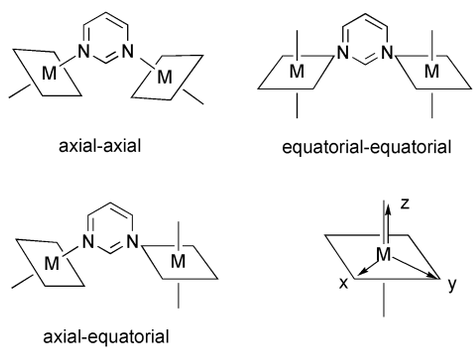

Scheme 1 Classification of coordination geometry for dinuclear pyrimidine complexes and definition of local *x,y,z* coordinates around a metal ion.

coordination was found in the latter complex. The extended Hückel molecular orbital calculation analysis suggests that the dσ–nσ orbital overlaps between copper $d_{x^2-y^2}$ and nitrogen n orbitals on both sides are related to an antiferromagnetic superexchange coupling across the PM ring.[25] The PM nitrogen atoms in **DPPM–Cu** are coordinated at the equatorial sites and the antiferromagnetic *J* value is comparable to those of the polynuclear complexes reported previously.[19,20] Compounds **DPPM–Mn**, **–Co**, and **–Ni** have axial–axial coordination geometries, and there are dσ–nσ orbital overlaps between d_{z^2} and nitrogen n orbitals on both sides.

Antiferromagnetic couplings in PM_2CoX_2 (X = Cl and Br)[26] and $PM{\cdot}Co[N(CN)_2]_2$[27] were also reported, but the coordination geometries are different; the PM nitrogen atoms are coordinated at axial positions in $PM{\cdot}Co[N(CN)_2]_2$ but at equatorial positions in PM_2CoX_2. The magnetic d_{z^2} and $d_{x^2-y^2}$ orbitals, both of which the high-spin (S = 3/2) cobalt ions usually possess, are available for dσ–nσ orbital overlap. As a consequence, the cobalt spins are antiferromagnetically correlated regardless of the coordination sites. Furthermore, for the isostructral nickel(II) derivatives, PM_2NiCl_2[28] and $PM{\cdot}Ni[N(CN)_2]_2$,[29] antiferromagnetic couplings observed can be interpreted likewise in terms of dσ–nσ-type orbital overlap. In view of a number of the experimental results obtained up to now, dσ–nσ orbital overlap on both sides of PM is concluded to favor antiferromagnetic coupling.

We performed *ab initio* and DFT molecular orbital calculations and found that the DFT results reproduced well the experimental results. Let us consider the shape of spin density distribution by graphical representation in order to explain and understand the conclusions described in the Results section. From Fig. 4 and Table 7, we find that Cu1 and coordinated nitrogen atoms (N1 and N2) carry spin densities with the same sign for all calculation methods. These spin structures can be interpreted in terms of the spin delocalization effect.[30] The spin delocalization effect in the Cu–N bond illustrates a resonance between Cu(↑)–N(↑↓) and Cu(↑↓)–N(↑) based on a ligand-to-metal charge transfer model, giving rise to the positive spin density on N. This situation shows a sharp contrast to those of organic high-spin materials bridged by *m*-phenylenes,[2] in which the spin density alternates throughout the π-conjugated hydrocarbon networks. It should be noted that the high-spin

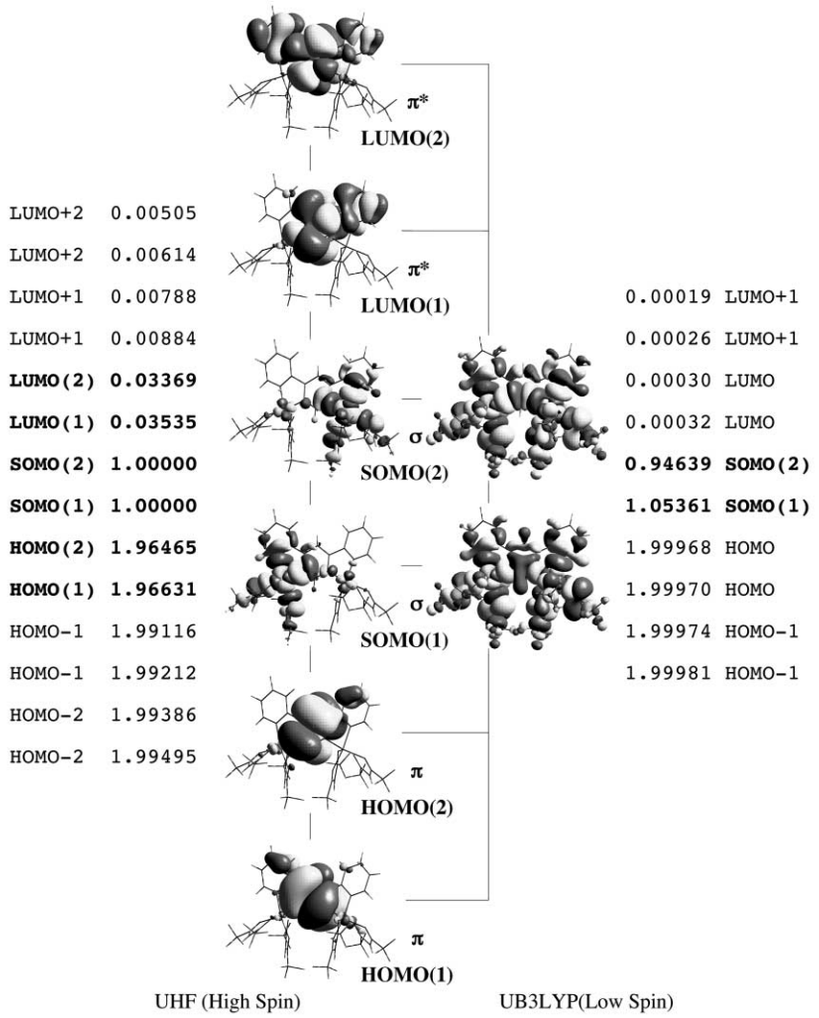

Fig. 5 Natural orbital coefficients and surfaces calculated by the UHF (left) and UB3LYP (right) methods for **DPPM–Cu**. Bold-faced natural orbitals appreciably contribute to the configuration interaction. For details of the calculations, see the text.

bisoxovanadium complex (**B**) showed a spin alternation in the V–PM–V skeleton, *i.e.*, the nitrogen atom carries a negative spin density[11] like the organic high-spin materials.

We also find that the UHF method gives much larger spin densities on the atoms of the ligand than the UB2LYP, UB3LYP and UBLYP methods. Furthermore, alternating spin densities on the PM ring are induced in the high-spin solution by UHF, whereas only nitrogen atoms (N2 and N3 in the PM bridge and N1 and N4 in the 2-pyridyl groups) in the ligand possess appreciable spin densities in the UB3LYP result.

Natural orbital[31] analysis for the **DPPM–Cu** molecules was carried out in order to study the contribution of frontier orbitals to the configuration interaction. The natural orbital coefficients for each orbital (highest-occupied molecular orbital (HOMO), singly-occupied molecular orbital (SOMO), lowest-unoccupied molecular orbital (LUMO) *etc.*) and their graphical representations for UHF (high-spin) and UB3LYP (low-spin) results are summarized in Fig. 5. The occupation numbers for SOMO(1) and SOMO(2) are close to unity and one electron occupies each orbital for both UHF and UB3LYP results. The lobes of these SOMOs spread not only over Cu atoms but also over their coordinated atoms through σ-bonds. In the case of UHF treatment two SOMOs and four other orbitals (HOMOs and LUMOs) must be taken into account in describing the configuration interaction, because the coefficients differ considerably from 2 or 0. The latter orbitals are localized on PM and possess a π-orbital nature. A π-pathway along N2–C9–N3 seems feasible for the magnetic interaction (Fig. 6(a)).

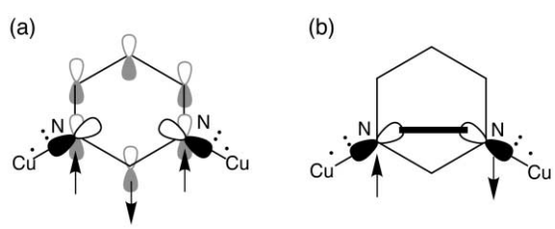

Fig. 6 Magnetic interaction paths. (a) Spin-polarization mechanism *via* π-bonds in the UHF calculation. The phase of $2p_z$ atomic orbitals are arbitrary. (b) Direct σ-type N ··· N interaction for the UB3LYP calculation. The lobes are drawn for the SOMO(1) case (Fig. 5).

On the other hand, only two SOMOs are essential to the configuration interaction for the UB3LYP solution. The two SOMOs have σ character. As the lobes of the SOMOs of UB3LYP show, a σ-pathway along Cu1–N2–N3–Cu2 can be proposed for the through-bond exchange mechanism (Fig. 6(b)). A similar direct N–N interaction has previously been proposed for the extended Hückel analysis of the PM-bridged copper(II) nitrate complex.[25] Therefore, the disagreement between the J_{ab} values obtained from the UHF and DFT calculations arises from overestimation of the π-type spin-polarization in the UHF treatment. As stated in the Introduction, the strategy realizing organic high-spin carbenes and radicals is based on π-spin-polarization,[2] and this strategy can not be applied for the present complex system.

Given that π-type spin-polarization effects should be negligible, we can propose a simplified rule which predicts the

role of magnetic couplers, using the Anderson–Goodenough–Kanamori theorem on the M_1–X–M_2 system.[32–34] When there is an appreciable orbital overlap between a magnetic orbital ϕ_1 on M_1 and an atomic orbital χ on X and at the same time there is also an overlap between χ and a magnetic orbital ϕ_2 on M_2, the spins of M_1 and M_2 are antiferromagnetically coupled. In the present complexes, the antiferromagnetic coupling is rationalized by assuming that χ is a molecular orbital of PM. The PM has local molecular orbitals consisting of $n_A + n_B$ and $n_A - n_B$, where n_A and n_B denote the lone pair of each nitrogen atom in PM, and no orthogonality is expected from the M_1–PM–M_2 system. Thus, the PM bridges work as antiferromagnetic couplers. This rule can also be applied to the PZ-bridged systems. Since the PZ has molecular orbitals $n_A + n_B$ and $n_A - n_B$ as well, the PZ bridge works as an antiferromagnetic coupler. In short, $\phi_1(d_{z^2}) \,//\, \chi \,//\, \phi_2(d_{z^2})$ and $\phi_1(d_{x^2-y^2}) \,//\, \chi \,//\, \phi_2(d_{x^2-y^2})$ bring about antiferromagnetic couplings for the axial–axial and equatorial–equatorial coordination geometries, respectively, where "//" denotes the presence of an orbital overlap. Only in the geometrically rare case of $\phi_1(d_{x^2-y^2}) \perp \chi \,//\, \phi_2(d_{x^2-y^2})$ for axial–equatorial coordination of some copper complexes, where "⊥" denotes the absence of any orbital overlap, does the PM bridge work as a ferromagnetic coupler.

The manganese(II) and cobalt(II) ions simultaneously have dπ and dσ spins. A detailed computational analysis of the simplest Mn–PM–Mn molecule with hypothetical hydride ligands has been reported recently.[30] The magnetic interaction is more complex because many kinds of magnetic interactions are present. As described above, after a positive spin density is polarized at the coordinated nitrogen atom, π- and σ-pathways may be operative which bring about ferro- and antiferromagnetic couplings, respectively. A σ-type spin-polarization pathway is also possible along the Mn–N–C–N–Mn bonded skeleton (not along the Mn–N ··· N–Mn shortcut), which may contribute as a ferromagnetic coupling term. When a negative spin polarization is assumed at the nitrogen atom using dπ spins as in the bisoxovanadium case,[11] possible ferromagnetic coupling contributes to the total interaction. In addition, symmetrical orthogonality suggests that the magnetic interaction of dπ–PM–dσ combination would be ferromagnetic, as clearly demonstrated for the bimetallic VO–Cu complexes.[35,36] Actually, the UB2LYP and UB3LYP calculations and UBLYP calculation on the hypothetical Mn–PM–Mn gave opposite solutions of J owing to a delicate balance.[30] The experimental results on **DPPM–** and **DPPZ–Mn** indicate that the antiferromagnetic contributions slightly surpass the ferromagnetic ones.

We found that the order of the absolute values of J for **DPPM–M** was J(Mn) < J(Co) < J(Ni) < J(Cu). The structural difference such as bond lengths of M1–N1 and M2–N3 should be taken into consideration. The observed order of J is consistent with the order of the M–N bond lengths (Table 4); shorter bond lengths bring about stronger interaction in general. We can propose another possible explanation, since typical dσ(d^9)–PMσ–dσ(d^9) and dπ(d^1)–PMπ–dπ(d^1) exchange pathways were clarified for **DPPM–Cu** and PM[VO(hfac)$_2$]$_2$,[11] respectively; the interaction in **DPPM–M** may be approximately explained by the balance between two major contributions from σ and π pathways. The observed magnetic interaction parameter J is expressed by the mean of the individual interactions J(i–j) between each unpaired electron (i) on one metal ion and each unpaired electron (j) on another metal ion.[37] Whereas the J(e_g–e_g) terms are antiferromagnetic as shown by **DPPM–Cu**, the J(t_{2g}–e_g) terms are ferromagnetic owing to orthogonality and the J(t_{2g}–t_{2g}) are also possibly ferromagnetic as clarified by PM[VO(hfac)$_2$]$_2$.[11] Taking the dinuclear Mn(II) complexes for example, only four terms are antiferromagnetic out of the total 25 terms. It is conceivable that the J values of **DPPM–M** positively shift with an increase of the number of magnetic t_{2g} orbitals.

Conclusion

We have clarified that both PM and PZ work as antiferromagnetic couplers in the dinuclear Mn^{II}, Co^{II}, Ni^{II} and Cu^{II} complexes and that the origin of the antiferromagnetic coupling is a superexchange through σ-bonds. For high-spin organic molecules using *m*-phenylene linkages the synthesis is laborious and perfect chemical transformation is difficult as the number of spins increases,[38] while pyrimidine-bridged transition-metal complexes have some advantages due to the nature of self-assembly. The present work suggests that metal ions with only dπ spins are potentially good candidates for developing pyrimidine-bridged magnets along this strategy.

Acknowledgements

This work was supported by Grant-in-Aid for Scientific Research on Priority Areas of "Molecular Conductors and Magnets" (No. 730/11224204) and by Grant-in-Aid for Scientific Research (No. 13640575) from the Ministry of Education, Culture, Sports, Science and Technology, Japan.

References and notes

1 O. Kahn, *Molecular Magnetism*, VCH, New York, 1993.
2 H. Iwamura, *Adv. Phys. Org. Chem.*, 1990, **26**, 179; A. Rajca, *Chem. Rev.*, 1994, **94**, 871; J. C. Longuet-Higgins, *J. Chem. Phys.*, 1950, **18**, 265; J. A. Crayston, J. N. Devine and J. C. Walton, *Tetrahedron*, 2000, **56**, 7829.
3 N. Mataga, *Theor. Chim. Acta*, 1967, **10**, 372; K. Matsuda, N. Nakamura, K. Takahashi, K. Inoue, N. Koga and H. Iwamura, *J. Am. Chem. Soc.*, 1995, **117**, 5550.
4 T. Ishida, S.-i Mitsubori, T. Nogami and H. Iwamura, *Mol. Cryst. Liq. Cryst.*, 1993, **233**, 345.
5 T. Ishida and T. Nogami, *Recent Res. Dev. Pure Appl. Chem.*, 1997, **1**, 1; T. Ishida, S.-i. Mitsubori, T. Nogami, Y. Ishikawa, M. Yasui, F. Iwasaki, H. Iwamura, N. Takeda and M. Ishikawa, *Synth. Met.*, 1995, **71**, 1791.
6 L. C. Francesconi, D. R. Corbin, A. W. Clauss, D. N. Hendrickson and G. D. Stucky, *Inorg. Chem.*, 1981, **20**, 2078.
7 V. A. Ung, S. M. Couchman, J. C. Jeffery, J. A. McCleverty, M. D. Ward, F. Totti and D. Gatteschi, *Inorg. Chem.*, 1999, **38**, 365.
8 H. Oshio and H. Ichida, *J. Phys. Chem.*, 1995, **99**, 3294; H. Oshio, *J. Chem. Soc., Chem. Commun.*, 1991, 240.
9 F. Lloret, G. De Munno, M. Julve, J. Cane, R. Ruiz and A. Caneschi, *Angew. Chem., Int. Ed.*, 1998, **37**, 135.
10 S.-i. Mitsubori, T. Ishida, T. Nogami and H. Iwamura, *Chem. Lett.*, 1994, 285; S.-I. Mitsubori, T. Ishida, T. Nogami, H. Iwamura, N. Takeda and M. Ishikawa, *Chem. Lett.*, 1994, 685.
11 T. Ishida, S.-i. Mitsubori, T. Nogami, N. Takeda, M. Ishikawa and H. Iwamura, *Inorg. Chem.*, 2001, **40**, 7059.
12 J. J. Lafferty and F. H. Case, *J. Org. Chem.*, 1967, **32**, 1591.
13 The composition formula of the **DPPM–M** crystals in ref. 4 should be corrected to **DPPM–M**·0.5C_6H_6.
14 teXsan: crystal structure analysis package, Molecular Structure Corp., The Woodlands, TX, 1985, 1999.
15 Gaussian98, M. J. Frisch, G. W. Trucks, H. B. Schlegel, G. E. Scuseria, M. A. Robb, J. R. Cheeseman, V. G. Zakrzewski, J. A. Montgomery, Jr., R. E. Stratmann, J. C. Burant, S. Dapprich, J. M. Millam, A. D. Daniels, K. N. Kudin, M. C. Strain, O. Farkas, J. Tomasi, V. Barone, M. Cossi, R. Cammi, B. Mennucci, C. Pomelli, C. Adamo, S. Clifford, J. Ochterski, G. A. Petersson, P. Y. Ayala, Q. Cui, K. Morokuma, D. K. Malick, A. D. Rabuck, K. Raghavachari, J. B. Foresman, J. Cioslowski, J. V. Ortiz, A. G. Baboul, B. B. Stefanov, G. Liu, A. Liashenko, P. Piskorz, I. Komaromi, R. Gomperts, R. L. Martin, D. J. Fox, T. Keith, M. A. Al-Laham, C. Y. Peng, A. Nanayakkara, C. Gonzalez, M. Challacombe, P. M. W. Gill, B. G. Johnson, W. Chen, M. W. Wong, J. L. Andres, M. Head-Gordon, E. S. Replogle and J. A. Pople, Gaussian, Inc., Pittsburgh, PA, 1998.
16 A. D. Becke, *J. Chem. Phys.*, 1993, **98**, 5648; A. D. Becke, *Phys. Rev. A*, 1988, **38**, 3098; C. Lee, W. Yang and R. G. Parr, *Phys. Rev. B*, 1988, **37**, 785.
17 Preliminary analysis of bond lengths of the low temperature phase of **DPPZ–Cu** measured at 100 K indicates that N2 and N3 are coordinated at the axial positions. The Cu1–N2 distance [2.175(8) Å] was longer than any other distances around Cu1 and the Cu2–N3

distance [2.360(7) Å] was also longer than any other distances around Cu2 at 100 K. No interaction between two Cu ions is rationalized by this structure. Selected crystallographic data are as follows: $C_{34}H_{14}N_4O_8F_{24}Cu_2$, T = 100 K, $P2_1/c$, a = 15.280(7), b = 17.349(6), c = 16.094(4) Å, β = 91.61(3)°, Z = 4, R = 0.0853 ($I > 2\sigma(I)$).
18 W. Wojciechowski, *Inorg. Chim. Acta*, 1967, **1**, 319.
19 M. Yasui, Y. Ishikawa, N. Akiyama, T. Ishida, T. Nogami and F. Iwasaki, *Acta Crystallogr., Sect. B*, 2001, **57**, 288; R. Feyerherm, S. Abens, D. Günther, T. Ishida, M. Meissner, M. Meschke, T. Nogami and M. Steiner, *J. Phys.: Condens. Matter*, 2000, **12**, 8495.
20 T. Ezuhara, K. Endo, K. Matsuda and Y. Aoyama, *New J. Chem.*, 2000, **24**, 609.
21 J. Omata, T. Ishida, D. Hashizume, F. Iwasaki and T. Nogami, *Inorg. Chem.*, 2001, **40**, 3954.
22 Y. Pontillon, A. Grand, T. Ishida, E. Leliévre-Berna, T. Nogami, E. Ressouche and J. Schweizer, *J. Mater. Chem.*, 2000, **10**, 1539.
23 G. Maruta, S. Takeda, R. Imachi, T. Ishida, T. Nogami and K. Yamaguchi, *J. Am. Chem. Soc.*, 1999, **121**, 424.
24 V. A. Reznikov, I. V. Ovcharenko, N. V. Pervukhina, V. N. Ikorskii, A. Grand and V. I. Ovcharenko, *Chem. Commun.*, 1999, 539; Y. Takano, Y. Kitagawa, T. Onishi, Y. Yoshioka, K. Yamaguchi, N. Koga and H. Iwamura, *J. Am. Chem. Soc.*, 2002, **124**, 450.
25 F. Mohri, K. Yoshizawa, T. Yamabe, T. Ishida and T. Nogami, *Mol. Eng.*, 1999, **8**, 357.
26 K. Nakayama, T. Ishida, R. Takayama, D. Hashizume, M. Yasui, F. Iwasaki and T. Nogami, *Chem. Lett.*, 1998, 497.
27 T. Kusaka, T. Ishida, D. Hashizume, F. Iwasaki and T. Nogami, *Chem. Lett.*, 2000, 1146.
28 K. Zusai, T. Kusaka, T. Ishida, R. Feryerherm, M. Steiner and T. Nogami, *Mol. Cryst. Liq. Cryst.*, 2000, **343**, 127.
29 T. Kusaka, T. Ishida, D. Hashizume, F. Iwasaki and T. Nogami, *Mol. Cryst. Liq. Cryst.*, 2002, **376**, 463.
30 Y. Takano, T. Onishi, Y. Kitagawa, T. Soda, Y. Yoshioka and K. Yamaguchi, *Int. J. Quantum Chem.*, 2000, **80**, 681.
31 K. Yamaguchi, M. Okamura, K. Takeda and S. Yamanaka, *Int. J. Quantum Chem., Quantum Chem. Symp.*, 1993, **27**, 501.
32 P. W. Anderson, *Phys. Rev.*, 1959, **115**, 2.
33 J. B. Goodenough, *Phys. Rev.*, 1955, **100**, 564.
34 J. Kanamori, *J. Phys. Chem. Solids*, 1959, **10**, 87.
35 N. Torihara, H. Okawa and S. Kida, *Chem. Lett.*, 1978, 1269.
36 O. Kahn, J. Galy, Y. Journaux, J. Jaud and I. Morgenstern-Badarau, *J. Am. Chem. Soc.*, 1982, **104**, 2165.
37 M. Ohba, H. Tamaki, N. Matsumoto and H. Okawa, *Inorg. Chem.*, 1993, **32**, 5385.
38 S. Rajca and A. Rajca, *J. Solid State Chem.*, 2001, **159**, 460; K. Matsuda, N. Nakamura, K. Inoue, N. Koga and H. Iwamura, *Bull. Chem. Soc. Jpn.*, 1996, **69**, 1483.